

Article

Improved Performance and Bias Stability of Al₂O₃/IZO Thin-Film Transistors with Vertical Diffusion

Se-Hyeong Lee, So-Young Bak and Moonsuk Yi *

Department of Electrical and Electronics Engineering, Pusan National University, Busan 46241, Korea; shlee19@pusan.ac.kr (S.-H.L.); bso6459027@pusan.ac.kr (S.-Y.B.)

* Correspondence: msyi@pusan.ac.kr; Tel.: +82-51-510-2381

Abstract: Several studies on amorphous oxide semiconductor thin-film transistors (TFTs) applicable to next-generation display devices have been conducted. To improve the poor switching characteristics and gate bias stability of co-sputtered aluminum–indium–zinc oxide (AIZO) TFTs, we fabricate Al₂O₃/indium–zinc oxide (IZO) dual-active-layer TFTs. By varying the Al₂O₃ target power and oxygen partial pressure in the chamber during Al₂O₃ back-channel deposition, we optimize the electrical characteristics and gate bias stability of the Al₂O₃/IZO TFTs. The Al₂O₃/IZO TFTs, which are fabricated under 50 W Al₂O₃ target power and 13% oxygen partial pressure conditions, exhibit a high electron mobility of 23.34 cm²/V·s, a low threshold voltage of 0.96 V, an improved on–off current ratio of 6.8 × 10⁷, and a subthreshold swing of 0.61 V/dec. Moreover, by increasing the oxygen partial pressure in the chamber, the positive and negative bias stress values improve to +0.32 V and −2.08 V, respectively. X-ray photoelectron spectroscopy is performed to reveal the cause of these improvements.

Keywords: amorphous oxide semiconductor; thin-film transistor; carrier suppressor; RF-magnetron sputtering; vertical diffusion



Citation: Lee, S.-H.; Bak, S.-Y.; Yi, M. Improved Performance and Bias Stability of Al₂O₃/IZO Thin-Film Transistors with Vertical Diffusion. *Electronics* **2022**, *11*, 2263. <https://doi.org/10.3390/electronics11142263>

Academic Editor: Antonio Di Bartolomeo

Received: 17 June 2022

Accepted: 12 July 2022

Published: 20 July 2022

Publisher's Note: MDPI stays neutral with regard to jurisdictional claims in published maps and institutional affiliations.



Copyright: © 2022 by the authors. Licensee MDPI, Basel, Switzerland. This article is an open access article distributed under the terms and conditions of the Creative Commons Attribution (CC BY) license (<https://creativecommons.org/licenses/by/4.0/>).

1. Introduction

Over the past few years, amorphous oxide semiconductors (AOS) such as amorphous indium–zinc oxide (a-IZO) have been studied extensively as channel layer materials for thin-film transistors (TFTs) because of their high electron mobility, transparency in visible light, uniformity of performance over a large area, and compatibility with flexible substrates. AOS TFTs are expected to be utilized in next-generation display devices, such as high-resolution, high-scanning-rate, flexible, and transparent devices [1–3]. High electron mobility is achieved because of the overlap of the s-orbitals of the metal, and electron carriers are supplied through the ionization of oxygen vacancies in the channel layer. However, a-IZO TFTs exhibit poor switching characteristics and voltage-bias stability because oxygen vacancies trap electron carriers. In amorphous indium–gallium–zinc oxide (a-IGZO), the most widely used AOS material in the channel layer of TFTs, the Ga cation improves the performance and bias stability by suppressing the generation of oxygen vacancies, which are traps in the channel layer and channel–insulator interface [4–6]. However, Ga is a rare earth element, and it is costly to be used for mass production. Several studies have been conducted to identify substitutes for expensive rare elements to resolve this cost limitation. Metal elements such as Ga, Al, Hf, and Zr have low electronegativity, standard electrode potential, and high metal–oxygen bonding energy [7–10]. These elements in the indium–zinc-based AOS channel layer, called carrier suppressors, form bonds with oxygen and suppress the generation of oxygen vacancies [11,12].

Because Al not only has a high metal–oxygen bonding energy but also has abundant reserves on Earth, we fabricated co-sputtered aluminum–indium–zinc oxide (AIZO) TFTs in a previous study. These devices exhibited good electrical performance and bias stability

but poor switching characteristics [13]. Because the radius of the Al cation is shorter than that of the In and Zn cations and equal to that of the Si cation, the Al cation easily migrates in the channel layer and serves as a trap defect at the channel–insulator interface [14–16]. In this work, to improve the switching characteristics and bias stability of AIZO TFTs, we fabricated AOS TFTs with an Al₂O₃/indium–zinc oxide (IZO) channel layer structure using vertical diffusion techniques [17,18]. By depositing an Al₂O₃ layer onto the IZO channel layer, the Al cations diffused into the IZO front-channel layer during the annealing process and suppressed the generation of oxygen vacancies. In addition, by varying the conditions of the Al₂O₃ back-channel deposition, such as the Al₂O₃ target power and oxygen partial pressure (OPP) in the chamber, we optimized the electrical characteristics and bias stability of the fabricated devices.

2. Materials and Methods

Inverted-staggered-type AIZO and Al₂O₃/IZO TFTs were fabricated using a heavily doped p-type Si substrate covered with thermally oxidized SiO₂ (150 nm thick). A p-type Si substrate and a SiO₂ layer were used as the gate electrode and gate insulator, respectively. First, as the reference channel layer, 25 nm amorphous AIZO layers were deposited onto the substrate at a room temperature of 25 °C using Al₂O₃ (with a purity of 99.99%) and IZO (In₂O₃: ZnO = 90 wt.%, 10 wt.%) targets via radio frequency (RF) magnetron co-sputtering. The Al₂O₃ target power was varied from 0 to 30 W in 10 W increments to confirm the effect of the Al cations in the channel layer. The IZO target power was fixed at 50 W, and the OPP [O₂/(Ar + O₂)] in the chamber was set to 13%.

The Al₂O₃/IZO channel layers were then deposited with a dual-layer structure as the experimental channel layer. At room temperature, a 20 nm IZO front-channel layer was deposited onto the substrate using the IZO target with 50 W power under 13% OPP via RF magnetron sputtering. An Al₂O₃ back-channel layer with less than 5 nm thickness was deposited onto the front-channel layer by applying power to the Al₂O₃ target under 13% OPP conditions via RF magnetron sputtering, increasing the power in 10 W steps from 20 to 50 W. This was performed to evaluate the effect of the Al₂O₃ back-channel target power on the electrical characteristics and gate bias stability of the fabricated TFTs. In addition, to verify the effect of the OPP condition in the chamber, we deposited an Al₂O₃ back-channel layer using an Al₂O₃ target with 50 W power under 13%, 20%, 25%, and 33% OPP conditions. During channel layer deposition, the initial pressure of the chamber was 3×10^{-6} Torr, and the process pressure was 2×10^{-3} Torr. In addition, all channel layers were patterned at $1000 \times 2000 \mu\text{m}$ using a shadow mask. After depositing the channel layers, annealing was performed using a hot plate at 250 °C for 1 h.

Next, 100 nm-thick Al was deposited using a shadow mask with a thermal evaporator to serve as the source/drain (S/D) electrodes. The fabricated TFTs had channel widths (W) and lengths (L) of 1000 and 100 μm , respectively. Figure 1 shows a schematic cross-section of the fabricated inverted-staggered-type (a) AIZO and (b) Al₂O₃/IZO TFTs. The electrical characteristics and bias stability of the fabricated TFTs were measured using an EL423 (ELESC) semiconductor parameter analyzer with two probes.

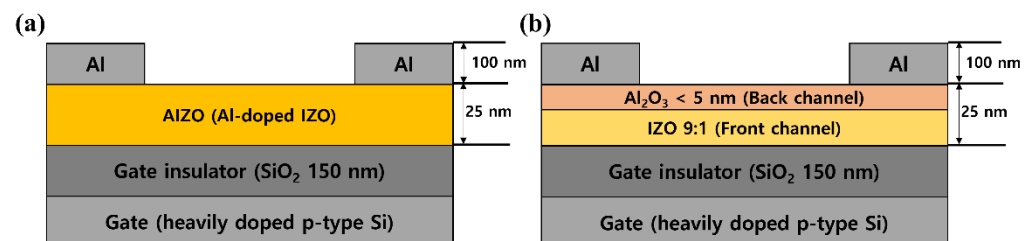


Figure 1. Schematic cross-section of inverted-staggered-type (a) AIZO and (b) Al₂O₃/IZO TFTs.

In addition, X-ray photoelectron spectroscopy (XPS) depth profiling analysis was performed to confirm the distribution of Al cations according to the depths in the AIZO and

Al₂O₃/IZO channel layers. Each XPS analysis was performed while dry etching the channel layers at intervals of 5 nm from the surface. The XPS measurements were performed using a monochromated Al K α X-ray source ($h\nu = 1486.6$ eV) at 15 kV/150 W. The spot size used was 400 μm (Theta Probe AR-XPS System, Thermo Fisher Scientific, Waltham, MA, USA). The O 1s spectra were deconvoluted into two peaks, centered at 530.1 ± 0.1 (OL) and 531.7 ± 0.1 eV (OH) [19,20].

3. Results and Discussion

Figure 2a and Table 1 show the transfer curves and electrical characteristic parameters of the co-sputtered AIZO TFTs, respectively, with respect to the Al₂O₃ target power. The AIZO 0 W (=pristine IZO) TFTs, which did not contain Al cations in the channel layer, exhibited poor electrical characteristics, except for high electron mobility. By increasing the Al₂O₃ target power during co-sputtering, the number of Al cations in the channel layer increased, suppressing the oxygen vacancy generation. Therefore, the electron mobility and off-current decreased slightly, and the threshold voltage shifted positively owing to the decreased carrier concentration and traps. Compared to the IZO TFTs, the AIZO TFTs exhibited improved bias stability. However, the optimized AIZO TFT with an Al₂O₃ target power of 20 W exhibited poor switching characteristics (=subthreshold swing) of 1.30 V/decade. The Al cations in the channel layer easily migrated to the channel–insulator interface and served as traps. However, in the Al₂O₃/IZO TFTs, the Al cations diffused into the IZO front-channel layer during annealing, which served as the buffer layer. The number of Al cations at the channel–insulator interface was significantly lower than that of AIZO TFTs.

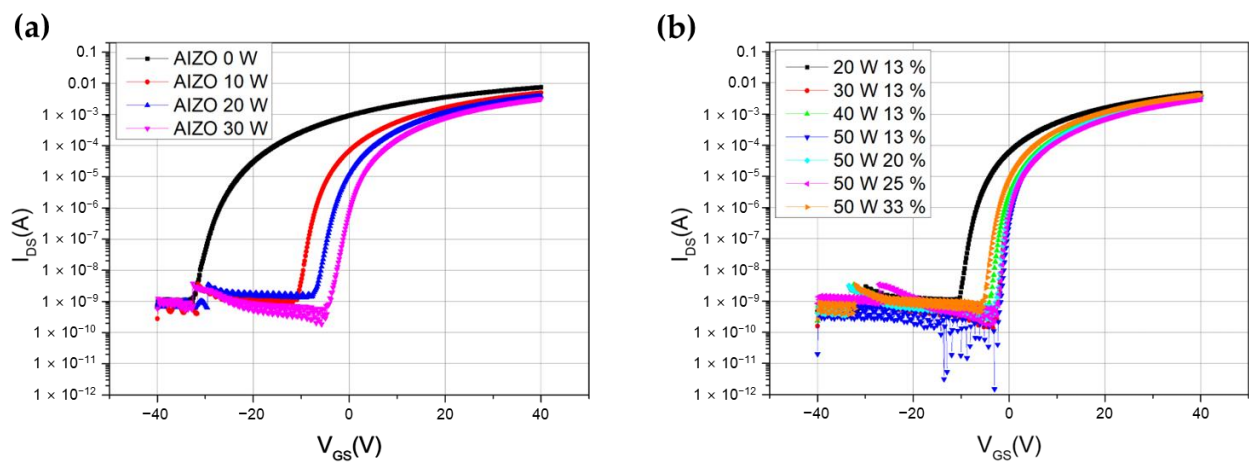


Figure 2. Transfer curves of (a) co-sputtered AIZO TFTs and (b) Al₂O₃/IZO TFTs according to Al₂O₃ target power and OPP in chamber.

Table 1. Electrical parameters of co-sputtered AIZO TFTs according to Al₂O₃ target power.

Al ₂ O ₃ Power (W)	μ_{sat} (cm ² /V·s)	V _{th} (V)	I _{on} /I _{off} Ratio	SS (V/Dec)
0 (Pristine IZO)	41.48	−26.88	9.8×10^6	1.44
10	27.25	−5.12	6.3×10^6	1.14
20	23.61	−0.96	2.9×10^6	1.30
30	22.29	0.96	1.1×10^7	1.29

Figure 2b and Table 2 show the transfer curves and electrical properties of the fabricated Al₂O₃/IZO TFTs according to the Al₂O₃ target power and OPP in the chamber, respectively. During Al₂O₃ back-channel deposition, the deposition rate increased in proportion to the Al₂O₃ target power. The Al₂O₃/IZO TFTs, fabricated using 20 W Al₂O₃ target power under the 13% OPP condition, exhibited worse characteristics than those under other conditions. This difference was attributed to the insufficient total amount of Al

cations diffused from the back channel to the front channel during annealing. However, this device exhibited relatively high electron mobility. This is because, as an insufficient amount of Al cations diffused into the IZO channel layer, the s-orbital overlap of indium and zinc cations was less disturbed compared to the other conditions [11–13]. The amount of Al cations diffused into the IZO front channel was increased by raising the Al₂O₃ target power while fixing the OPP to 13% to improve the electrical characteristics of the fabricated TFTs. As the target power increased, the on–off current ratio (I_{on}/I_{off}) and subthreshold swing (SS) improved significantly. In addition, it was confirmed that the saturation mobility (μ_{sat}) was maintained above 20 cm²/V·s, and the threshold voltage (V_{th}) positively shifted to near 0 V.

Table 2. Electrical parameters of Al₂O₃/IZO TFTs according to Al₂O₃ target power and OPP in chamber.

Al ₂ O ₃ Power (W)	OPP (%)	μ_{sat} (cm ² /V·s)	V_{th} (V)	I_{on}/I_{off} Ratio	SS (V/Dec)
20	13	26.44	−5.76	6.6×10^6	1.01
30	13	23.04	0.96	7.3×10^6	1.00
40	13	21.16	0.16	7.9×10^6	0.80
50	13	23.34	0.96	6.8×10^7	0.61
50	20	21.94	1.12	1.2×10^7	0.70
50	25	19.81	1.6	1.2×10^7	0.69
50	33	24.49	−0.8	6.3×10^6	0.86

Because the co-sputtered AIZO channel layer, which was deposited using an IZO (In: Zn = 90 wt.%: 10 wt.%) target, exhibited optimal performance when the OPP in the chamber was 13%, there existed limitations to improving the electrical properties by changing the OPP conditions. However, in the Al₂O₃/IZO channel structure, as the IZO front-channel layer was first deposited under 13% OPP, the Al₂O₃ back-channel layer was deposited by varying the OPP in the chamber. To verify the effect of the OPP in the chamber during Al₂O₃ back-channel deposition, we analyzed the electrical properties of the fabricated Al₂O₃/IZO TFTs by fixing the target power to 50 W and increasing the OPP in the chamber (Figure 2b and Table 2). As the OPP increased, the carrier mobility decreased slightly, the threshold voltage shifted in the positive direction, the on–off current ratio was approximately 10⁷, and the SS values ranged between 0.6 and 0.7 V/dec. Without this tendency, the electrical characteristics of the fabricated TFTs deteriorated when the OPP was 33%. When the OPP was increased under an identical process pressure, the number of Ar atoms in the chamber and the sputtering rate decreased; therefore, the Al₂O₃ back-channel layer contained an insufficient amount of Al cations.

Finally, we fabricated improved Al₂O₃/IZO TFTs with 50 W Al₂O₃ target power and 13% OPP in the chamber during back-channel deposition. In Figure 3, we denote the pristine IZO TFTs, Al-doped IZO TFTs with 20 W Al₂O₃ target power, and Al₂O₃/IZO TFTs with 50 W Al₂O₃ target power under the 13% OPP condition as “AIZO 0 W”, “AIZO 20 W”, and “Al₂O₃/IZO Dual Layer”, respectively. The results show that the Al₂O₃/IZO TFTs exhibited a high electron carrier mobility of 23.34 cm²/V·s and a low threshold voltage of 0.96 V. In particular, compared to AIZO 20 W TFTs, the SS value representing the switching characteristics of TFTs decreased by more than 53% to 0.61 V/dec, and the on–off current ratio increased by more than 20 times to 6.8×10^7 . Therefore, in the fabricated Al₂O₃/IZO TFTs, compared to the co-sputtered AIZO TFTs, the electrical properties were adjusted by varying the Al₂O₃ target power and the OPP during back-channel deposition. The switching characteristics, which are the disadvantages of conventional AIZO TFTs, were improved, and a high on–off current ratio was obtained.

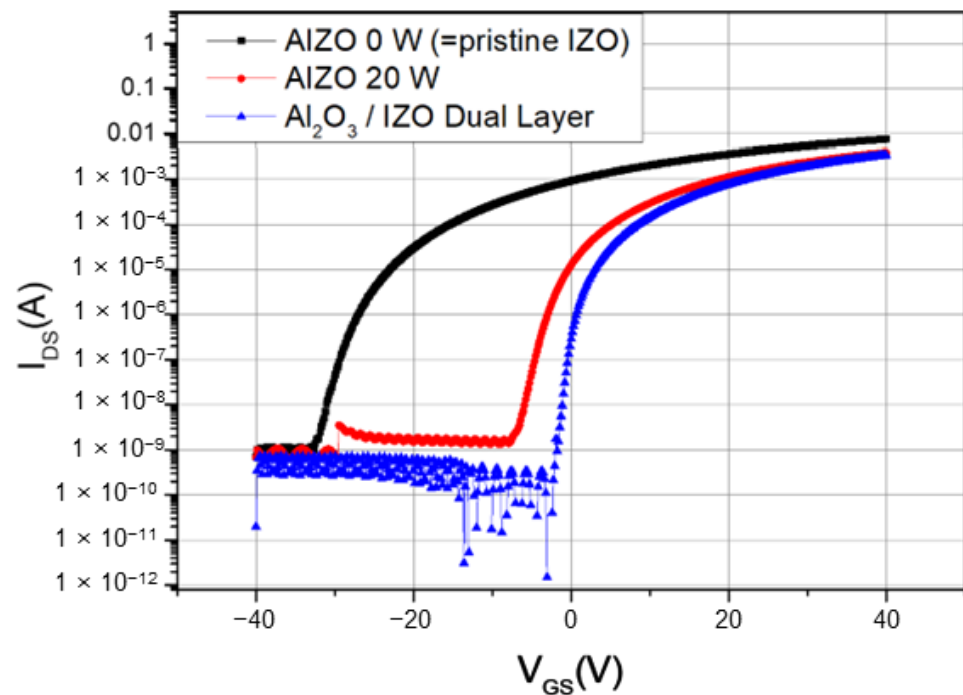


Figure 3. Transfer curves of AIZO 0 W (Al_2O_3 target power = 0 W, OPP = 13%), AIZO 20 W (Al_2O_3 target power = 20 W, OPP = 13%), and Al_2O_3 /IZO Dual Layer (Al_2O_3 target power = 50 W, OPP = 13%) TFTs.

However, the gate bias stability of the Al_2O_3 /IZO TFTs fabricated with 50 W Al_2O_3 target power and 13% OPP was degraded compared to that of the AIZO 20 W TFTs. Positive bias stress ($V_{\text{GS}} = +10$ V, $V_{\text{DS}} = 0$ V, PBS) and negative bias stress ($V_{\text{GS}} = -10$ V, $V_{\text{DS}} = 0$ V, NBS) were applied to the AIZO 20 W and Al_2O_3 /IZO TFTs at room temperature under ambient conditions for 3600 s, respectively, to investigate the gate bias stability of the fabricated TFTs. During the PBS test, the AIZO 20 W and Al_2O_3 /IZO TFTs showed a threshold voltage shift of approximately +1 V, exhibiting relatively good gate bias stability. However, during the NBS test, the AIZO 20 W and Al_2O_3 /IZO TFTs showed threshold voltage shifts of -3.36 and -4.96 V, respectively, indicating poor gate bias stability. The PBS test results were better than the NBS test results because the AIZO 20 W and Al_2O_3 /IZO channel layers had more traps in the back channel than in the channel–insulator interface [21,22]. To improve the gate bias stability of the Al_2O_3 /IZO TFTs under NBS, we reduced the oxygen vacancies in the back channel and analyzed the threshold voltage shift by varying the Al_2O_3 target power and OPP in the chamber during back-channel deposition in Figure 4. Under 13% OPP, all the NBS results were poor because of numerous oxygen vacancies in the back-channel layer (Figure 4a). In contrast, under 20% OPP, the NBS results improved as the Al_2O_3 target power increased, and the best results were obtained at 50 W target power. The NBS results improved as the target power increased because the Al cations in the back-channel increased, and the traps on the surface decreased. Because the applied power limit of the two-inch Al_2O_3 target was 60 W, the target power was applied from 0 to 50 W in 10 W increments.

To further improve the gate bias stability under NBS, we analyzed the threshold voltage shift according to the OPP in the chamber during back-channel deposition while fixing the Al_2O_3 target power to 50 W (Figure 4b). Below 20% OPP, the NBS results improved as the OPP increased, and the NBS threshold voltage shift under 20% OPP showed the lowest value of -2.08 V. As the OPP increased during back-channel deposition, the number of oxygen vacancies on the surface decreased. Above 20% OPP, the NBS results deteriorated as the OPP increased up to 33%. As explained earlier (Figure 2), the number of Ar atoms in the chamber and the sputtering rate of the Al_2O_3 target decreased with increasing OPP under an identical process pressure. Therefore, the Al cations in the

back-channel were insufficient in suppressing oxygen vacancy generation. Based on the electrical performance and gate bias stability, optimized Al₂O₃/IZO TFTs were fabricated with an Al₂O₃ target power of 50 W and 20% OPP during back-channel deposition. The PBS and NBS results of the AIZO 20 W and optimized Al₂O₃/IZO TFTs are presented in Figure 5 and Table 3. The optimized Al₂O₃/IZO TFTs exhibited better gate bias stability than the AIZO 20 W TFTs under PBS and NBS. The PBS and NBS results improved from +1.44 to +0.32 V and −3.36 to −2.08 V, respectively.

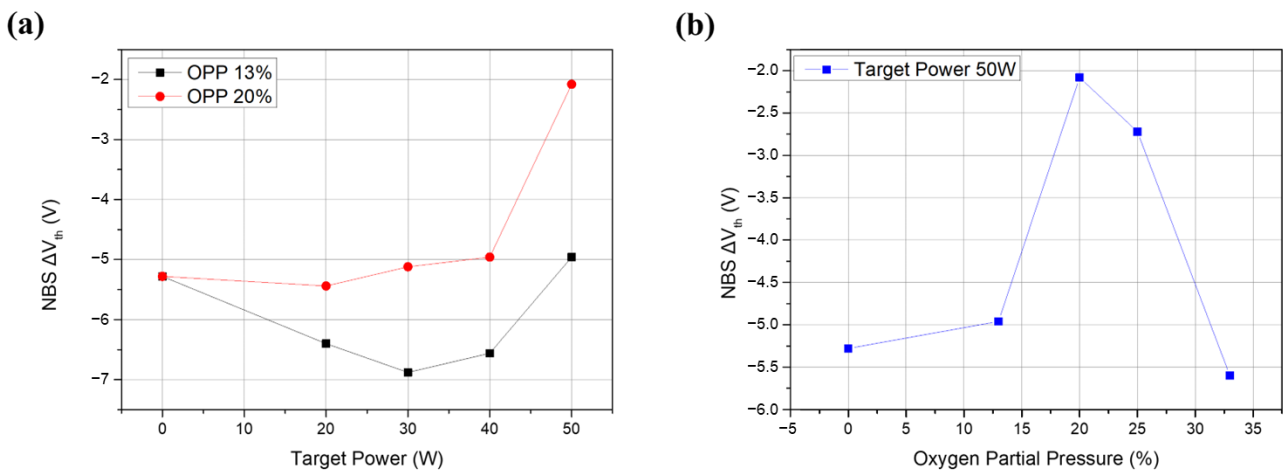


Figure 4. Comparison of NBS results according to (a) Al₂O₃ target power and (b) OPP.

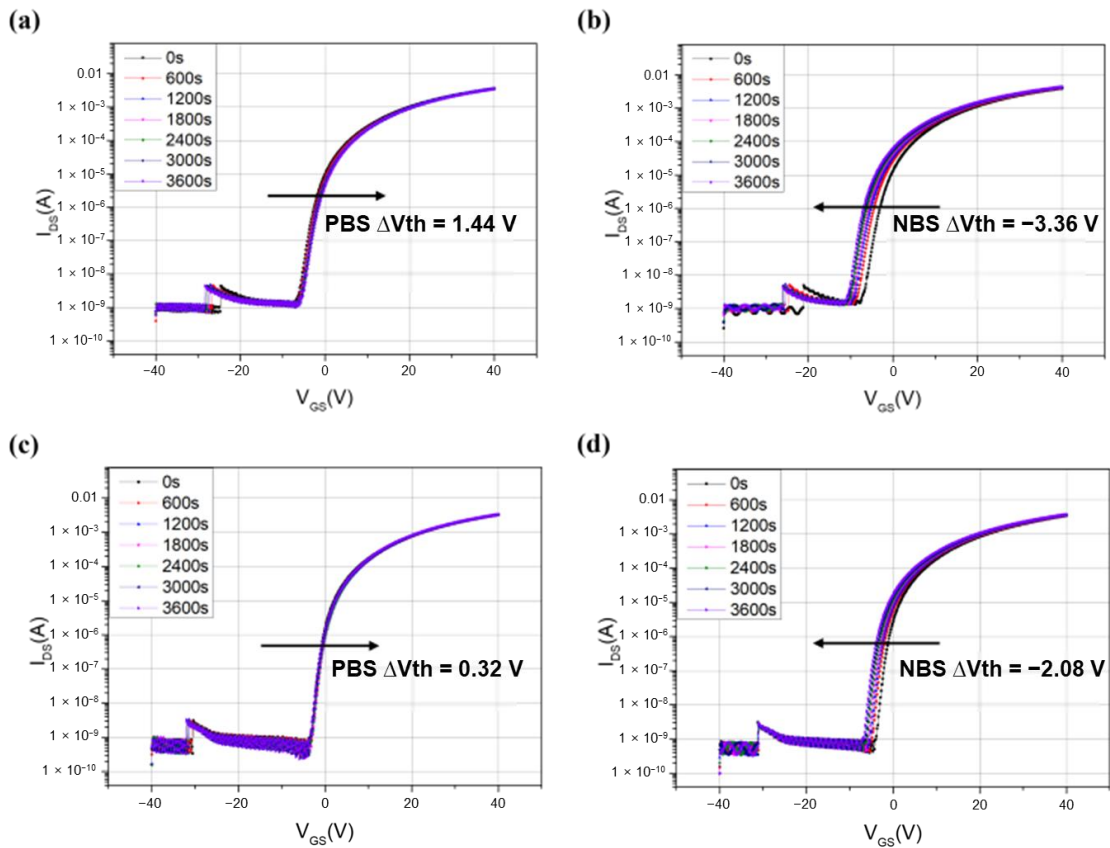


Figure 5. Gate bias stress results for AIZO and Al₂O₃/IZO TFTs for varying stress durations: (a) PBS: AIZO 20 W, (b) NBS: AIZO 20 W, (c) PBS: Al₂O₃/IZO 50 W OPP 20%, and (d) NBS: Al₂O₃/IZO 50 W OPP 20%.

Table 3. V_{th} shifts in AIZO and Al_2O_3 /IZO TFTs under PBS and NBS conditions (over 3600 s).

Type of Stress	AIZO TFT ($Al_2O_3 = 20\text{ W}$)	Al_2O_3 /IZO TFT ($Al_2O_3 = 50\text{ W}$, OPP = 20%)
ΔV_{th} of PBS (V)	+1.44	+0.32
ΔV_{th} of NBS (V)	−3.36	−2.08

To investigate the effect of the Al_2O_3 /IZO channel structure on electrical performance and gate bias stability, we performed an XPS depth profiling analysis to investigate the chemical bonding states according to the depths in the active-channel layers of the AIZO 20 W and optimized Al_2O_3 /IZO TFTs (Al_2O_3 target power: 50 W, OPP: 20%). Al cations, the carrier suppressors, exist in about 1 wt.% in the channel layers. Their chemical composition is very small, so it is difficult to directly measure them [13]. Therefore, in the XPS depth profiling results, we tried to indirectly confirm the distribution of Al cations, the carrier suppressors, by showing changes in oxygen binding states according to the depths of the AIZO and Al_2O_3 /IZO channel layers. The results are presented in Figure 6 and Table 4. The lower binding energy peak area (O_L) in red and the higher binding energy peak area (O_H) in blue are related to the oxygen anions present in the metal–oxide bonds (M–O bonds) and the metal oxide lattice with oxygen vacancies (V_O), respectively [19,20].

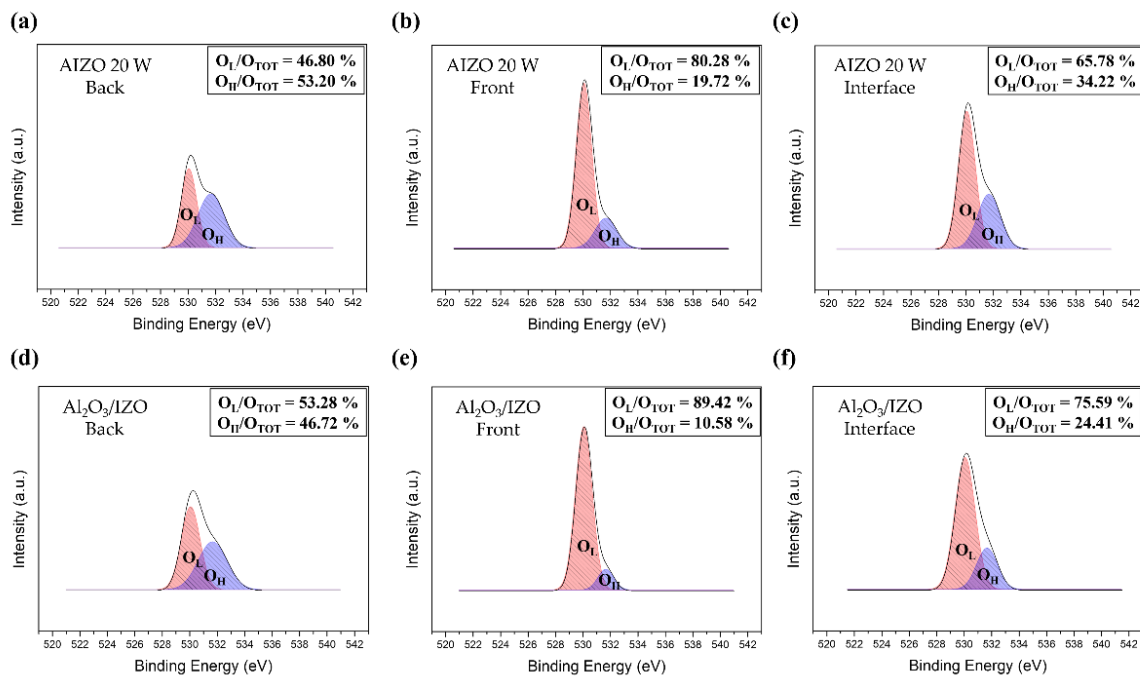


Figure 6. XPS of O 1s region in (a) AIZO 20 W back channel, (b) AIZO 20 W front channel, (c) AIZO 20 W channel–insulator interface, (d) Al_2O_3 /IZO 50 W OPP 20% back channel, (e) Al_2O_3 /IZO 50 W OPP 20% front channel, and (f) Al_2O_3 /IZO 50 W OPP 20% channel–insulator interface.

Table 4. XPS analysis results for AIZO and Al_2O_3 /IZO TFTs according to channel layer depth.

Depth of channel	AIZO TFT ($Al_2O_3 = 20\text{ W}$)		Al_2O_3 /IZO TFT ($Al_2O_3 = 50\text{ W}$, OPP = 20%)	
	O_H/O_{TOT}	O_L/O_{TOT}	O_H/O_{TOT}	O_L/O_{TOT}
0 nm (Back channel)	53.20%	46.80%	46.72%	53.28%
10 nm (Front channel)	19.72%	80.28%	10.58%	89.42%
20 nm (Channel–insulator interface)	34.22%	65.78%	24.41%	75.59%

The back channel, front channel, and channel–insulator interface indicated that the active-channel layer was located at depths of 0, 10, and 20 nm from the surface, respectively. In the front channel and channel–insulator interface, the Al₂O₃/IZO TFTs showed a lower ratio of the OH peak area to the total-binding energy peak area (OTOT) than the AIZO 20 W TFTs, as shown in Figure 6b,c,e,f. These results demonstrate that the Al₂O₃/IZO channel layer has chemical bonds with fewer oxygen vacancies than the co-sputtered AIZO channel layer. Therefore, the fabricated Al₂O₃/IZO TFTs exhibited improved switching characteristics, a high on–off current ratio, and good gate bias stability under PBS. In addition, for the back channel results, the co-sputtered AIZO channel layer showed a higher OH/OTOT peak area ratio than the OL/OTOT peak area ratio. This suggests that the number of M–O bonds is fewer than that of the oxygen vacancies on the back-channel surface, as shown in Figure 6a. However, the Al₂O₃/IZO had a lower OH/OTOT peak area ratio than the OL/OTOT peak area ratio (Figure 6d). These results indicate that the Al₂O₃/IZO channel layer, in which the back channel was deposited at 50 W Al₂O₃ target power under 20% OPP, had fewer oxygen vacancies on the back-channel surface than the co-sputtered AIZO channel layer, exhibiting an improved gate bias stability under NBS. From the XPS results, we confirmed that the Al₂O₃/IZO channel structure suppressed the oxygen vacancies in the entire range of the channel layer compared to the AIZO channel layer, improving the electrical performance and gate bias stability.

4. Conclusions

We fabricated AOS TFTs with an Al₂O₃/IZO channel structure to improve the switching characteristics and gate bias stability of the co-sputtered AIZO TFTs while maintaining excellent electrical performance. In the co-sputtered AIZO channel layer, the Al cations acted as traps at the channel–insulator interface and deteriorated the switching characteristics. In the Al₂O₃/IZO channel layer, Al cations diffused into the front channel from the back channel during annealing by separately depositing the IZO front channel and the Al₂O₃ back channel such that relatively few Al cations existed at the channel–insulator interface. In addition, the electrical characteristics and gate bias stability of the Al₂O₃/IZO TFTs were improved by varying the target power and OPP conditions in the chamber during Al₂O₃ back-channel deposition. Based on the electrical characteristics only, the Al₂O₃/IZO TFTs, which were fabricated under 50 W Al₂O₃ target power and 13% OPP conditions, exhibited a high electron mobility (μ_{sat}) of 23.34 cm²/V·s and a low threshold voltage (V_{th}) of 0.96 V. Compared to the co-sputtered AIZO TFTs, the subthreshold swing, which indicates the switching characteristics, and the on–off current ratio improved significantly by more than 53% (0.61 V/dec) and 20 times (6.8×10^7), respectively. However, for the NBS test results, the Al₂O₃/IZO TFTs fabricated under the 13% OPP condition exhibited a high threshold voltage shift. Therefore, considering the gate bias stability with a slight decrease in the electrical performance, the optimized Al₂O₃/IZO TFTs were fabricated under 50 W Al₂O₃ target power and 20% OPP conditions. Compared to the co-sputtered AIZO TFTs, the threshold voltage shift of the PBS and NBS decreased from +1.44 to +0.32 V and –3.36 to –2.08 V, respectively.

Author Contributions: Conceptualization, experiments, and writing—original draft preparation, S.-H.L.; writing—review and editing, S.-Y.B.; supervision, M.Y. All authors have read and agreed to the published version of the manuscript.

Funding: This study was supported by BK21PLUS, Creative Human Resource Education and Research Programs for ICT Convergence in the 4th Industrial Revolution. This study was supported by a National Research Foundation of Korea (NRF) grant funded by the Korean government (MSIT) (No. 2021R1A4A102708711). This study was supported by Korea Institute for Advancement of Technology (KIAT) grant funded by the Korea Government (MOTIE) (G02P07820002113, The Competency Development Program for Industry Specialist).

Institutional Review Board Statement: Not applicable.

Informed Consent Statement: Not applicable.

Data Availability Statement: Not applicable.

Conflicts of Interest: The authors declare no conflict of interest.

References

1. Nomura, K.; Ohta, H.; Takagi, A.; Kamina, T.; Hirano, M.; Hosono, H. Room-temperature fabrication of transparent flexible thin-film transistors using amorphous oxide semiconductors. *Nature* **2004**, *432*, 488–492. [[CrossRef](#)] [[PubMed](#)]
2. Kamina, T.; Nomura, K.; Hosono, H. Present status of amorphous In-Ga-Zn-O thin-film transistors. *Sci. Technol. Adv. Mater.* **2010**, *11*, 044305. [[CrossRef](#)] [[PubMed](#)]
3. Park, J.S.; Maeng, W.J.; Kim, H.S.; Park, J.S. Review of recent developments in amorphous oxide semiconductor thin-film transistor devices. *Thin Solid Films* **2012**, *520*, 1679–1693. [[CrossRef](#)]
4. Lee, D.H.; Park, S.M.; Kim, D.K.; Lim, Y.S.; Yi, M. Effects of Ga composition ratio and annealing temperature on the electrical characteristic of solution processed IGZO thin-film transistors. *J. Semicond. Technol. Sci.* **2014**, *14*, 163–168. [[CrossRef](#)]
5. Lee, S.Y.; Chang, S.; Lee, J.S. Role of high-k gate insulators for oxide thin-film transistors. *Thin Solid Films* **2010**, *518*, 3030–3032. [[CrossRef](#)]
6. Jeong, S.; Ha, Y.G.; Moon, J.; Facchetti, A.; Marks, T.J. Role of gallium doping in dramatically lowering amorphous-oxide processing temperatures for solution-derived indium zinc oxide thin-film transistors. *Adv. Mater.* **2009**, *22*, 1346–1350. [[CrossRef](#)] [[PubMed](#)]
7. Chen, K.Y.; Yang, C.C.; Su, Y.K.; Wang, Z.H.; Yu, H.C. Impact of oxygen vacancy on the photo-electrical properties of In₂O₃-based thin-film transistor by doping Ga. *Materials* **2019**, *12*, 737. [[CrossRef](#)]
8. Sun, J.; Huang, Y.; Gong, H. Improved mobility and conductivity of an Al₂O₃ incorporated indium zinc oxide system. *J. Appl. Phys.* **2011**, *110*, 023709. [[CrossRef](#)]
9. Lee, D.; Choi, P.; Park, A.; Jeon, W.; Choi, D.; Lee, S.; Choi, B. Hafnium incorporation in InZnO thin-film transistors as a carrier suppressor. *J. Nanosci. Nanotechnol.* **2020**, *20*, 6675–6678. [[CrossRef](#)]
10. Zhang, J.; Fu, X.; Zhou, S.; Ning, H.; Wang, Y.; Guo, D.; Cai, W.; Liang, Z.; Yao, R.; Peng, J. The effect of zirconium doping on solution-processed indium oxide thin films measured by a novel nondestructive testing method (microwave photoconductivity decay). *Coatings* **2019**, *9*, 426. [[CrossRef](#)]
11. Parthiban, S.; Kwon, J.Y. Role of dopants as a carrier suppressor and strong oxygen binder in amorphous indium-oxide based field effect transistor. *J. Mater. Res.* **2014**, *29*, 1585–1596. [[CrossRef](#)]
12. Kim, G.H.; Jeong, W.H.; Ahn, B.D.; Shin, H.S.; Kim, H.J.; Kim, H.J.; Ryu, M.K.; Park, K.B.; Seon, J.B.; Lee, S.Y. Investigation of the effects of Mg incorporation into InZnO for high-performance and high-stability solution-processed thin-film transistors. *Appl. Phys. Lett.* **2010**, *96*, 163506. [[CrossRef](#)]
13. Park, J.; Lim, Y.; Jang, M.; Choi, S.; Hwang, N.; Yi, M. Improved stability of aluminum co-sputtered indium zinc oxide thin-film transistor. *Mater. Res. Bull.* **2017**, *96*, 155–159. [[CrossRef](#)]
14. Li, Y.; Lan, L.; Xiao, P.; Lin, Z.; Sun, S.; Song, W.; Song, E.; Gao, P.; Wang, D.; Ning, H.; et al. Solution-processed indium-zinc-oxide thin-film transistors based on anodized aluminum oxide gate insulator modified with zirconium oxide. *RCS Adv.* **2015**, *5*, 51440–51445. [[CrossRef](#)]
15. Li, L.J.; Deng, H.; Dai, L.P.; Chen, J.J.; Yuan, Q.L.; Li, Y. Properties of Al heavy-doped ZnO thin films by RF magnetron sputtering. *Mater. Res. Bull.* **2008**, *43*, 1456–1462. [[CrossRef](#)]
16. Lee, C.T.; Lin, Y.H.; Lin, J.H. High stability mechanisms of quinary indium gallium zinc aluminum oxide multicomponent oxide films and thin-film transistors. *J. Appl. Phys.* **2015**, *117*, 045309. [[CrossRef](#)]
17. Yoon, S.; Kim, S.J.; Tak, Y.J.; Kim, H.J. A solution-processed quaternary oxide system obtained at low-temperature using a vertical diffusion technique. *Sci. Rep.* **2017**, *7*, 43216. [[CrossRef](#)]
18. Lee, S.H.; Lee, S.; Woo, K.; Kim, Y.J.; Bak, S.Y.; Han, Y.J.; Kim, S.; Han, T.H.; Yi, M. Effects of thermal annealing time and molar ratio of channel layers on solution-processed ZnO/SnO₂ thin-film transistors. *Solid-State Electron.* **2020**, *165*, 107765. [[CrossRef](#)]
19. Chen, M.; Pei, Z.L.; Sun, C.; Wen, L.S.; Wang Jr, X. Surface characterization of transparent conductive oxide Al-doped ZnO films. *J. Cryst. Growth* **2000**, *220*, 254–262. [[CrossRef](#)]
20. Fan, J.C.C.; Goodenough, J.B. X-ray photoemission spectroscopy studies of Sn-doped indium-oxide films. *J. Appl. Phys.* **1977**, *48*, 35524. [[CrossRef](#)]
21. Shiah, Y.-S.; Sim, K.; Shi, Y. Mobility–stability trade-off in oxide thin-film transistors. *Nature Electron.* **2021**, *4*, 800–807. [[CrossRef](#)]
22. Shian, Y.-S.; Sim, K.; Ueda, S.; Kim, J.; Hosono, H. Unintended Carbon-Related Impurity and Negative Bias Instability in High-Mobility Oxide TFTs. *IEEE Electron Device Lett.* **2021**, *42*, 1319–1322.